arXiv:1511.05596v2 [cond-mat.mes-hall] 3 May 2016

Multi-domain electromagnetic absorption of triangular quantum rings

Anna Sitek[1,2], Gunnar Thorgilsson[3], Vidar Gudmundsson[1], and Andrei Manolescu[3]

[1]Science Institute, University of Iceland, Dunhaga 3, IS-107 Reykjavik, Iceland
[2]Department of Theoretical Physics, Faculty of Fundamental Problems of Technology, Wroclaw University of Technology, 50-370 Wroclaw, Poland
[3]School of Science and Engineering, Reykjavik University, Menntavegur 1, IS-101 Reykjavik, Iceland

Abstract

We present a theoretical study of the unielectronic energy spectra, electron localization, and optical absorption of triangular core-shell quantum rings. We show how these properties depend on geometric details of the triangle, such as side thickness or corners' symmetry. For equilateral triangles, the lowest six energy states (including spin) are grouped in an energy shell, are localized only around corner areas, and are separated by a large energy gap from the states with higher energy which are localized on the sides of the triangle. The energy levels strongly depend on the aspect ratio of the triangle sides, i.e., thickness/length ratio, in such a way that the energy differences are not monotonous functions of this ratio. In particular, the energy gap between the group of states localized in corners and the states localized on the sides strongly decreases with increasing the side thickness, and then slightly increases for thicker samples. With increasing the thickness the low-energy shell remains distinct but the spatial distribution of these states spreads. The behavior of the energy levels and localization leads to a thickness dependent absorption spectrum where one transition may be tuned in the THz domain and a second transition can be tuned from THz to the infrared range of electromagnetic spectrum. We show how these features may be further controlled with an external magnetic field. In this work the electron-electron Coulomb repulsion is neglected.

1 Introduction

Polygonal quantum rings are nanoscale structures with diameters from tens to hundreds of nanometers and lateral thickness down to few nanometers [1]. Such structures may be achieved due to the possibility of combining two or more different materials into one vertical structure, i.e., core-shell nanowires. They contain a core, itself a quantum wire, which is covered by one or more layers of different materials. Due to the variety of controllable physical properties core-shell nanowires have recently turned out to be suitable building blocks of many quantum nanodevices such as solar cells [2, 3], nanoantennas [4], field-effect transitions [5, 6], lasers [7], including plasmon lasers [8], light-emitting diodes [9], THz radiation sources [10] and detectors [11].

One of the physical properties which may be modeled during the growth process is band alignment. Core-shell nanowires are built of at least two different materials, each one having its own energy structure, which changes considerably in the presence of strain [12]. In most cases core and shell materials have different lattice constants, and thus the combined system differs substantially from the bulk of each component, or from single material nanowires, and depends on the geometrical details. This provides a possibility to control band alignment through the core and shell thicknesses [13, 14] and thus to achieve systems in which conduction electrons may be found only in the shell area [15]. The present art of manufacturing allows for etching the core part such that the remaining shell forms a nanotube of finite thickness [16, 17]. If such nanowires are sufficiently short, i.e., of height much smaller that the radius, then they may be considered as quantum rings, as long as only the lowest wave-function mode in the growth direction is relevant.

Physical properties of polygonal quantum rings differ considerably from their circular counterparts. Electrons are always equally distributed along the whole circumference of homogeneous circular structures, while in the case of polygonal systems the localization pattern is much more complicated. As in the case of bent quantum wires [18], in the corners of polygonal rings effective quantum wells are formed, with energy levels determined by the size and shape of the area between internal and external polygon boundaries. This results in localization of low energy electrons in the vicinity of corners, whereas carriers associated with higher energy levels are purely or partly localized in side areas [19, 20]. In the absence of external fields the ground state of circular rings is twofold (spin) degenerate while all exited states are fourfold (spin and orbital momentum)

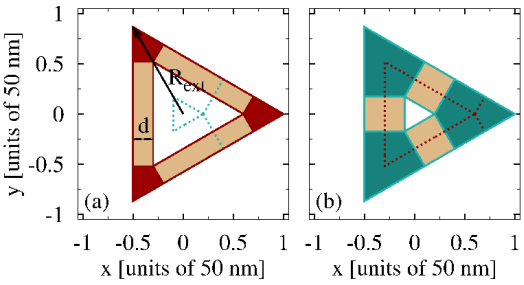

Figure 1: Ring model: Symmetric samples restricted internally and externally by equilateral triangles. We keep the external radii constant and equal $R_{\rm ext} = 50$ nm and change the side thickness d. In Fig. (a) $d = 10$ nm and in Fig. (b) $d = 20$ nm. The areas included between the internal and external boundaries where effective quantum wells are formed are marked in red or turquoise. Doted turquoise and red lines indicate internal boundaries and corner areas of 20 (a) and 10 nm (b) thick samples.

degenerate. In the case of polygonal rings the ground state is also twofold degenerate, but higher levels are either two- or fourfold degenerate and the degeneracy pattern is determined by the number of corners [21]. Depending on the ring shape, corner-localized states may be separated from side-localized ones by an energy gap [20].

In this paper we show how the spectral properties of the single electron states confined in triangular quantum rings depend on the geometric aspect ratio, i.e., the ratio between the lateral thickness and the side length, or, equivalently, the radius of a circle encompassing the ring. We show how corner localization maxima merge with increasing side thickness and define conditions under which low energy electrons are expelled from side areas. The ground state energy and splittings between consecutive levels depend on the ring's shape. The energy gap separating corner- from side-localized states may reach high values for thin triangular samples and may be tuned within a wide energy range. As a result the rings absorb photons of distinct energies which may be controlled to high extent.

The paper is organized as follows. In the next section we define the sample model and describe the methods we use in our calculations. In Sec. 3 we show our results, in particular we investigate how energy levels and carrier localization change with the aspect ratio between the side thickness and sample radii for the case of equilateral rings (Sec. 3.1) and non-symmetric samples (Sec. 3.2). Next we show how those features are reflected in the absorption spectrum, Sec. 3.3. The summary and final remarks are contained in Sec. 4.

2 The model

All analyzed rings are restricted externally by equilateral triangles, with a fixed radius $R_{\rm ext} = 50$ nm, i.e., the distance from the center to the corners, but variable side thickness, such that the core area is varied, as illustrated in Fig. 1. The quantum states were obtained with two different computational methods, based on discretization of the Schrödinger equation on polar and triangular grids, respectively.

In the method based on the polar grid we start with a disk of radius $R_{\rm ext}$ discretized in polar coordinates [22]. The triangular samples are achieved by imposing polygonal boundaries within the disk, and excluding from the grid all sites situated outside those boundaries. We have recently used this method to describe various polygonal rings [20]. In the position representation the Hilbert space is spanned by vectors $|kj\sigma\rangle$, where the indexes k and j correspond to discretized radial $r = r_k$ and angular $\phi = \phi_j$ coordinates, separated by intervals δr and $\delta\phi$, and σ is the spin projection on the z direction. The kinetic Hamiltonian matrix elements defined on the polar grid are

$$H^K_{kj\sigma,k'j'\sigma'} = T\delta_{\sigma,\sigma'}\left[t_r\left(\delta_{k,k'} - \delta_{k,k'+1}\right)\delta_{j,j'} + t_\phi\delta_{k,k'}\left(\delta_{j,j'} - \delta_{j,j'+1}\right) + \text{H.c.}\right], \tag{1}$$

where $T = \hbar^2/(2m^*R^2_{\rm ext})$ is the reference energy, m^* the electron mass in the ring material, $t_r = (R_{\rm ext}/\delta r)^2$, and $t_\phi = [R_{\rm ext}/(r_k\delta\phi)]^2$. We assume that the ring is immersed in an external static magnetic field B perpendicular to the plane of the ring, i.e., associated with the vector potential $\boldsymbol{A} = B(-y, x, 0)/2$. The corresponding Hamiltonian matrix elements are

$$H^B_{kj\sigma,k'j'\sigma'} = T\delta_{\sigma,\sigma'}\delta_{k,k'}\left[\frac{1}{2}t_{\rm B}^2\left(\frac{r_k}{4R_{\rm ext}}\right)^2\delta_{j,j'} - t_{\rm B}\frac{i}{4\delta\phi}\delta_{j,j'+1} + \text{H.c.}\right],$$

with $t_{\rm B} = \hbar eB/m^*T$ being the cyclotron energy in units of T. Finally, we take into account the Zeeman

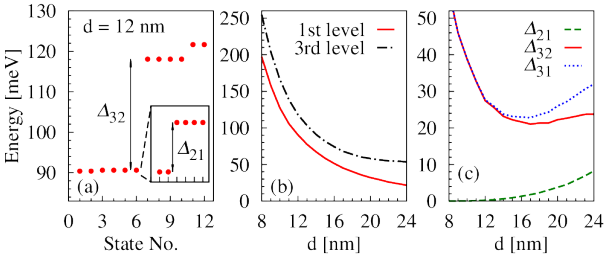

Figure 2: Energy levels of equilateral triangular quantum rings. (a) The four lowest energy levels of 12 nm thick sample and their degeneracy, the two lowest levels are repeated in the inset. (b) Ground state and the third energy level changing with side thickness. (c) Energy gap dependence on side thickness: energy splitting between the two levels associated with corner-localized probability distributions, Δ_{21}, an energy gap separating corner- from side-localized states, Δ_{32}, and the energy difference between the third energy level and the ground state, Δ_{31}.

effect which results in splitting of spin degenerate energy levels. For the relevant Hamiltonian we obtain

$$H^{\mathrm{Z}}_{kj\sigma,k'j'\sigma'} = \frac{1}{2} T t_{\mathrm{B}} \gamma \left(\sigma_z\right)_{\sigma,\sigma'} \delta_{k,k'} \delta_{j,j'}, \tag{2}$$

where $\gamma = g^* m^*/2m_e$ is the ratio between the Zeeman gap and the cyclotron energy, and m_e is the free electron mass. The total Hamiltonian is thus $H = H^K + H^B + H^Z$. We use material parameters of InAs which are the effective mass $m^* = 0.023 m_e$ and the effective g-factor $g^* = -14.9$.

In the second method the software package KWANT [23] was used to construct the Hamiltonian matrix elements of the system. The system was discretized on an equilateral triangular grid. This scheme allowed for an equally dense grid over the whole triangular quantum ring, together with a good representation of the corners. The eigenenergies and eigenvectors of the resulting Hamiltonian matrix where calculated using a linear algebra package.

The numerical calculations on the (nonuniform) polar grid were performed using around 6900 grid points and between 2000-12000 in the case of the KWANT software. We used both computational methods to explore the dependence of the energy levels and wave functions on side thickness, and since both methods predicted very similar behavior we present only the results obtained with the polar grid.

3 Results and discussion

Below we show our results on the geometry dependent properties of triangular quantum rings. We start our discussion from symmetric (equilateral) samples with constant external radii and show how their energy levels and electron localization change with increasing side thicknesses. In the next step we analyze the electron energies and localization for the case of non-symmetric rings. Finally, we show how those features affect the absorption spectrum.

3.1 Energy structure and carrier localization of symmetric rings

The energy levels of polygonal quantum rings show a unique degeneracy pattern which depends only on the number of corners [20, 21]. In the case of symmetric (restricted internally and externally by regular triangles) rings and zero magnetic field the ground state is twofold (spin) degenerate, the second and third levels are fourfold (spin and orbital momentum) degenerate and the fourth level is again twofold degenerate, Fig. 2(a). The ground state energy and the gaps between consecutive levels depend on the aspect ratio of the triangle. If the external radius is assumed to be constant then the ground state energy changes as the inverse of squared side thickness [red solid line in Fig. 2(b)]. But the evolution of the third energy level [the black dashed dotted line in Fig. 2(b)] is more complicated: it decreases relatively fast for thin rings and slows down for thicker samples. In Fig. 2(c) we show the energy intervals between the three pairs of levels. The energy gap in the corner state domain, i.e., between the ground state and the first excited state, Δ_{21}, increases with side thickness [the green dashed line in Fig. 2(c)]. The next energy gap, Δ_{32}, which separates corner- from side-localized states, initially decreases with the thickness until it reaches a minimum value for the aspect ratio of around 0.34, and then it starts increasing slightly [the red solid line in Fig. 2(c)]. The sum of those two energy gaps makes up a splitting between the ground state and the third energy level, Δ_{31} [the blue dotted line in Fig. 2(c)], which differs considerably from the main energy gap Δ_{32} only for thick samples

where the contribution from the splitting of the two lowest levels is substantial. In particular the minimum of Δ_{31} occurs for a thickness only slightly smaller than for Δ_{32}.

The mentioned features may be explained with a closer look at the geometry of the corner areas. In Fig. 1 we compare two rings which are externally restricted by identical equilateral triangles but have different side thicknesses, 10 nm in Fig. 1(a) and 20 nm in Fig. 1(b), respectively. As can be seen, the corner areas between the internal and external boundaries, where effective quantum wells are formed, increase with ring thickness. Since quantum well energy levels scale with the squared inverse of their size, the decrease of the ground state energy shown in Fig. 2(b) may be understandable.

The localization pattern also changes with increasing side thickness, Fig. 3, but low-energy electrons are always attracted by the corner quantum wells. The number of corner-localized states equals to the double number of corners (if spin degeneracy is included) which means that probability distributions associated with the two lowest levels (two- and fourfold degenerate) of triangular rings form maxima in that areas [20]. In the case of narrow rings the ground state is localized over very small areas in the corners, where sharp and high localization peaks are formed, and the probability distribution vanishes along the whole side length, Fig. 3(a).

The corner areas increase with side thickness (Fig. 1) and the ground state localization maxima decrease, becoming spread over much larger areas, and penetrating into the sides. For sufficiently thick samples, i.e., for aspect ratio around 0.24, the localization peaks begin merging in the middle of the sides, Figs. 3(b)–3(d). Similar effects occur for the corner-localized probability distributions associated with the second energy level, Figs. 3(e)–3(h), but corner maxima become even sharper with increasing energy, and thus the probability of finding electrons from the second energy level in the middle of the sides increases much slower compared to the case of the ground state. The thicker is the ring the larger is the difference between localization patterns associated with the two lowest levels which results in higher energy splitting between the corresponding energy levels [the green dashed line in Fig. 2(c)].

According to our definition, thick rings are built around very narrow cores. For the 24 nm thick sample shown in Figs. 3(d), 3(h), and 3(l) the core radius equals 2 nm. The side thickness of 25 nm corresponds to a full triangle. The ground state probability distribution for a full triangle forms one, relatively wide, peak in the middle of the sample. The localization pattern shown in Fig. 3(d) is split into three half merging maxima situated close to the center, i.e., looking like the ground state probability distribution of a full triangle pierced in the middle. The first excited state of a full triangle, which incorporates shorter wavelengths, forms sharper maxima shifted towards the corners. The difference of the probability distributions associated with the first and second energy levels of wider triangular rings can be understood by analogy with the full triangle. The result is that the localization peaks in the ground state are (slightly) broader than in the first excited state.

In the case of sufficiently thin samples the probability distribution associated with the first value above the corner-localized domain, i.e., the third energy level, is distributed between all of the sides of symmetric samples and forms a maximum in the middle of each side [20]. This localization shape changes with thickness in the opposite way to the ground state localization pattern, Figs. 3(i)- 3(l). As seen in Fig. 1, the thicker is the ring the larger is the ratio of the corner to side areas [red or turquoise to beige areas in Fig. 1]. This results in sharper and higher side maxima which need to adjust to relatively smaller localization space. Interestingly, for thicker rings purely side-localized states do not occur and the probability distribution associated with the first level above the corner-localized domain forms sharp maxima in the middle of the sides, which may be even higher than the peaks associated with the second energy level, and are accompanied by lower corner maxima, Figs. 3(k) and 3(l).

The most interesting characteristic feature of triangular rings is the large energy gap separating states with qualitatively different probability distributions, in the corner areas, or in the middle of the sides. Analog corner and side localization occurs for square and hexagonal rings, but in those cases the energy separating such states is much smaller than for triangles [20]. In the discussion of Fig. 3, these localization patterns change in opposite ways with increasing side thickness, i.e. the difference between them becomes less pronounced, which corresponds to the decrease of the energy gap. For thick rings the probability distribution associated with the third energy level forms six maxima, i.e., again the localization patterns start to differ more and thus the energy gap increases slightly.

3.2 Energy structure and carrier localization of non-equilateral rings

Many properties of polygonal quantum rings are very sensitive to the sample symmetry. Energy levels of non-symmetric triangular rings are only twofold (spin) degenerate. Still, probability distributions associated with the six lowest states, now arranged into three levels, are localized in corner areas. Contrary to the previous case they are not equally distributed between all of the corners but may be localized on single ones [20]. In Fig. 4 we show the energies of non-equilateral triangular samples for which the thickness of one side has been increased by 4% and of a second one by 8% with respect to the third side. As can be seen in Fig. 4(a) the

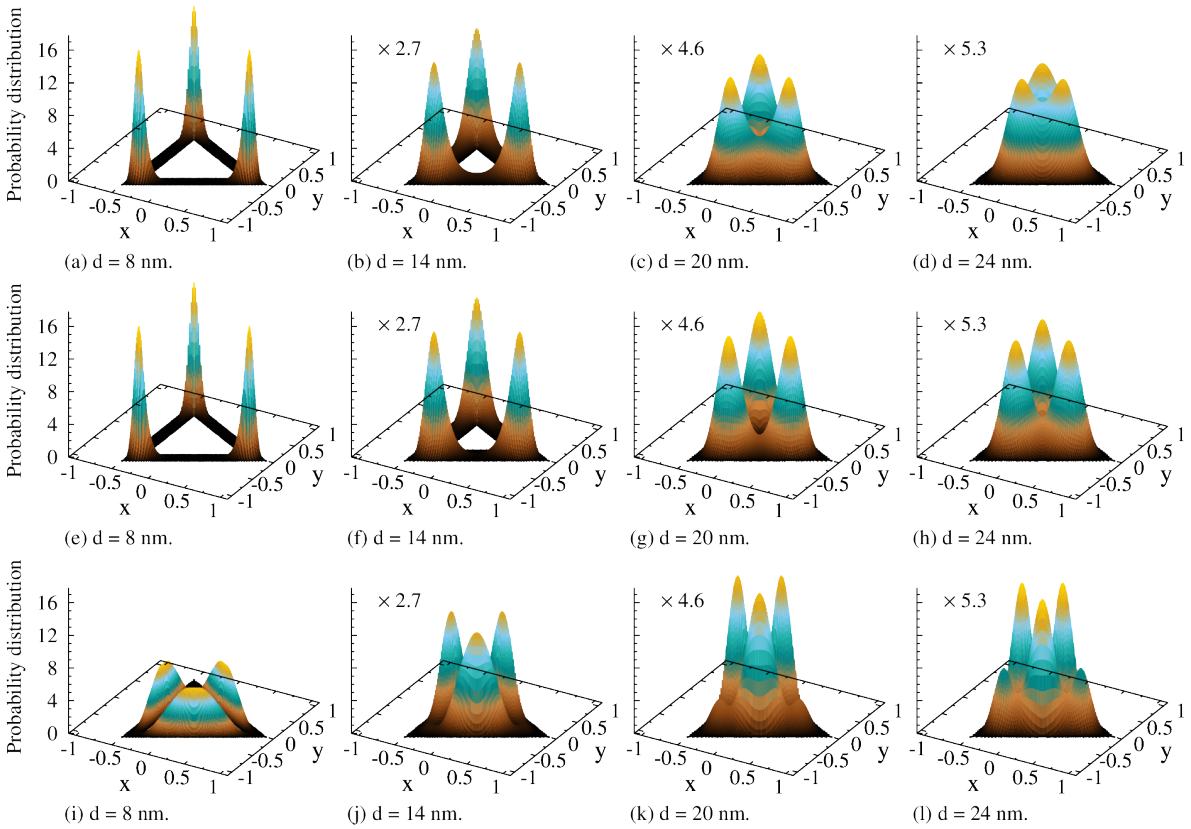

Figure 3: Probability distribution associated with the ground state (a-d), the second energy level (e-h) and the third level (i-l) for symmetric triangular rings of different side width d. The x and y coordinates are in units of R_{ext} and probability distribution in units of R_{ext}^{-2}. The distributions for d=8 nm are taken as reference, and for the other cases they are magnified with factors shown on the top left corner of each graph.

energy levels of the thicker sample resemble much more the ones of equilateral ring [Fig. 2(a)] than the energy structure of the thinner sample. This can be understood if one takes a look once again on the geometry of corner areas. If the ring sides have different thicknesses then the areas contained between internal and external boundaries differ from each other which leads to formation of three quantum wells of different depth within one ring. In the case of narrower samples the ratio between corner areas is much higher than in the case of thicker rings, this results in substantially different quantum well in each corner and thus also energy spectrum and carrier localization do not resemble the ones of equilateral triangles. With increasing ring thickness the ratios between corner areas decrease and thus the difference between non-symmetric samples and equilateral rings becomes less pronounced and their properties similar. The positions of the ground state and exited levels as well as splittings between them change similarly to the case of equilateral triangles with only small shape dependent deviations [Fig. 4(b) and 4(c)], but the corresponding probability distributions differ considerably from the previously analyzed case. Irrespective of the aspect ratio the levels built of the six lowest states are separated from the higher ones by an energy gap and associated with corner-localized probability distributions while electrons occupying higher levels may be more easily found in the sides. Contrary to the symmetric samples, if the rings are sufficiently thin then, single localization peaks are formed in both corner and side areas. The deepest quantum well is formed in the corner for which the area between internal and external boundaries is the largest and thus the ground state electrons are localized in that corner [Fig. 5(a)]. The probability distribution associated with the second energy level forms a single peak around the medial corner area. Finally, the shallower quantum well is situated in the smallest corner whose ground state corresponds to the third energy level of the system and thus electrons excited to this level occupy the corner for which the area between the boundaries is the smallest [Fig. 5(e)]. Also the three side areas differ from each other and the probability distribution associated with the first levels above the gap forms a single maximum in the largest side area [Fig. 5(i)] while electrons excited to the two following levels occupy the two other sides, respectively. With increasing side thickness the ratio between the depth of the three quantum wells decreases which results in delocalized probability distributions and increasing number of localization peaks. For the geometry presented here probability distributions associated with the two lowest levels first form a single peak in the largest corner then two maxima at the ends of the thickest side and finally also a small maximum

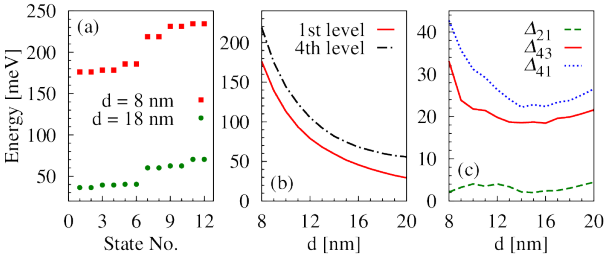

Figure 4: Energy levels of non-symmetric triangular rings. (a) The six lowest energy levels and their degeneracy for two samples with aspect ratios equal to 0.16 ($d = 8$ nm) and 0.36 ($d = 18$ nm), respectively. (b) Ground state and the fourth level changing with side thickness. (c) Energy gap dependence on side thickness: energy splitting between the two lowest levels associated with corner localized probability distributions, Δ_{21}, an energy gap separating corner- and side-localized states, Δ_{43}, and the energy difference between the fourth (mostly side-localized level) and the ground state, Δ_{41}. The values of the side thickness shown in Fig. (a) and on the axises of Figs. (b) and (c) refer to the thickness of the narrowest side.

in the third corner [Fig. 5(a)- 5(d)]. Electrons excited to the third level practically occupy only the smallest corner but with very small probabilities they may also be found in the other corners of very thick samples [Fig. 5(e)- 5(h)]. Localization patterns corresponding to the levels above the gap form one main peak in the widest side which is accompanied by two smaller peaks in the other sides of thick rings [Fig. 5(i)- 5(l)]. As a result thicker non-symmetric rings resemble much more their equilateral counterparts and due to smaller differences between the effective quantum wells it is much easier to control them externally, i.e., to achieve properties similar to equilateral counterparts as well as to thin non-symmetric rings.

3.3 Electromagnetic absorption

We calculate the absorption coefficient using the formula [24, 12, 25]

$$\alpha(\hbar\omega) = \mathcal{A}\hbar\omega \sum_{\mathrm{f}} |\langle f|\boldsymbol{\varepsilon}\cdot\boldsymbol{d}|i\rangle|^2 \delta\left(\hbar\omega - (E_{\mathrm{f}} - E_{\mathrm{i}})\right), \tag{3}$$

where $\mathcal{A}$ is a constant amplitude depending on the ring's properties, $\boldsymbol{\varepsilon} = (1, \pm i)/\sqrt{2}$ the circular polarization of an electromagnetic field (defined with respect to the ring's plane), $\boldsymbol{d}$ the dipole moment, and $E_{\mathrm{i,f}}$ the initial and final energies, respectively. The dipole matrix elements depend on the eigenstates and thus are sensitive to the sample geometry,

$$\langle f|\boldsymbol{\varepsilon}\cdot\boldsymbol{d}|i\rangle = \frac{1}{\sqrt{2}} \sum_{q} \Psi^{\dagger}(q,f)\,\Psi(q,i)\,r_k\left(\cos\phi_j \pm i\sin\phi_j\right).$$

Here q stands for the basis states ($|q\rangle \equiv |kj\sigma\rangle$) and $\Psi(q,a)$ are the amplitudes of the eigenvector $|a\rangle$ of the triangular ring in the q basis, $|a\rangle = \sum_q \Psi(q,a)\,|q\rangle$.

The δ (Dirac) function is approximated by a Lorentzian,

$$\delta\left(\hbar\omega - (E_{\mathrm{f}} - E_{\mathrm{i}})\right) \approx \frac{\Gamma/2}{\left[\hbar\omega - (E_{\mathrm{f}} - E_{\mathrm{i}})\right]^2 + (\Gamma/2)^2},$$

where $\Gamma/2$ is a phenomenological broadening of the discrete energy levels of the samples and is fixed to 0.028 meV. This value allows for a sufficient energy resolution for analyzing particular transitions. In practice this broadening may have complex physical origin, from all possible imperfections of the core-shell structure, but a proper modeling of it is beyond the scope of the present work.

The absorption spectrum is governed by the intervals between the energy levels, $E_f - E_i$, and by the dipole selection rules, incorporated in Eq. (3). Since the energy levels strongly depend on side thickness or aspect ratio, the absorption of core-shell rings may be established during the manufacturing process. It can be further tuned with an external magnetic field perpendicular to the plane of the polygon, which lifts both spin and orbital degeneracies. As a result the four degenerate energy levels shown in Fig. 2(a) become twelve non-degenerate levels with energies depending on the field strength. In Fig. 6 we compare energy intervals between the ground state and the eleven excited states (around which maxima of the gray dotted lines are formed) and absorption spectra (the green solid and red dashed lines) of a 12 nm symmetric quantum ring obtained for three different strengths of the magnetic field.

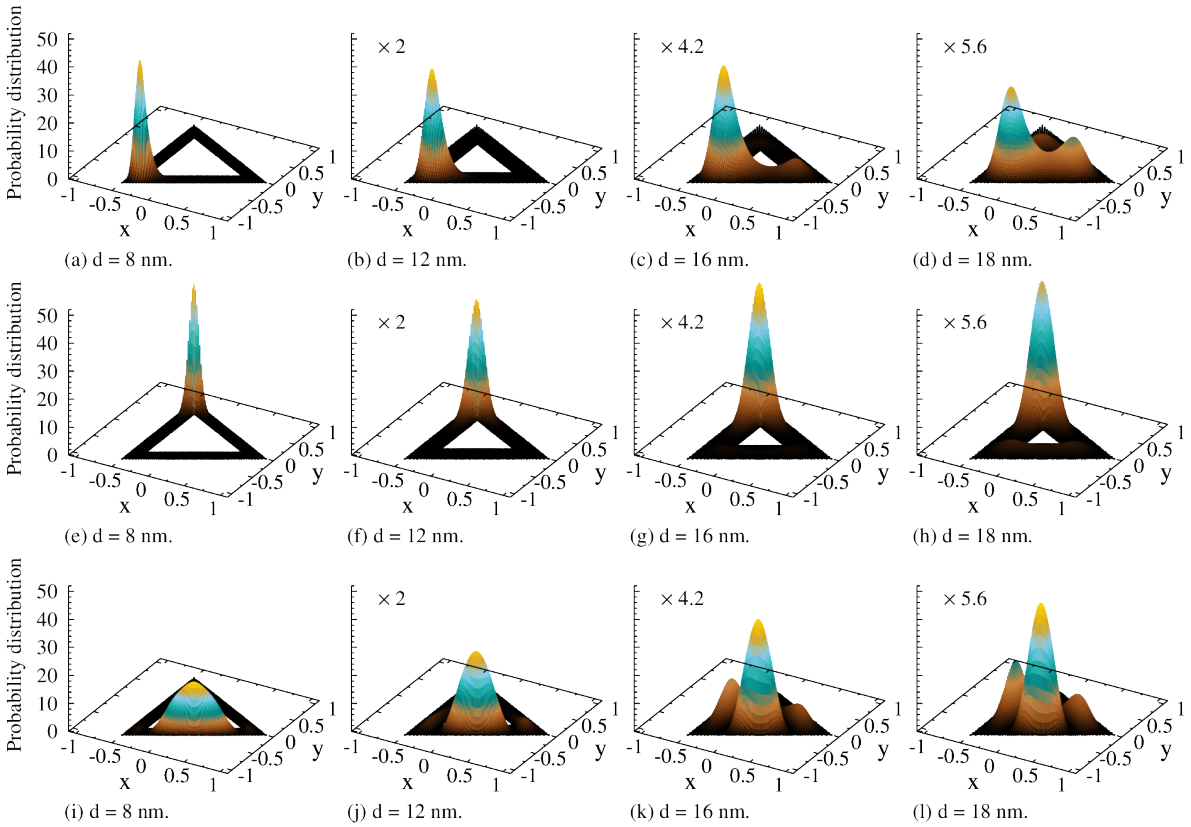

Figure 5: Probability distribution associated with the ground state (a-d), the third energy level (e-h) and the fourth one (i-l) for non-symmetric samples. The samples were restricted externally by the same equilateral triangles for which $R_{\text{ext}} = 50$ nm while the internal boundaries were defined by different side thicknesses. The values of the side thickness shown in the figure captions refer to the sides parallel to lines $y = (-x + 1)/\sqrt{3}$, the thicknesses of the two other sides were increased by 4% (sides parallel to the y axis) and 8% (sides parallel to line $y = (x - 1)/\sqrt{3}$) with respect to the shown values. The x and y coordinates are in units of R_{ext} and probability distribution in units of R_{ext}^{-2}. The distributions for $d = 8$ nm are taken as reference, and for the other cases they are magnified with factors shown on the top left corner of each graph.

If a symmetric polygonal ring containing an electron in its ground state is exposed to a clockwise polarized light then the electron can be excited to one of the corner-localized or to one of the side-localized states. The spin direction is conserved in the absence of spin-orbit coupling. Two different transitions occur in the presence of the counterclockwise polarized electromagnetic field, such that in total the ground state electron may be excited to four different states, two belonging to corner-localized domain [Figs. 6(a), 6(c) and 6(e)] and the other two to side-localized one [Figs. 6(b), 6(d) and 6(f)] [20]. As can be seen in Fig. 6, the positions of absorption maxima change with the magnetic field on the single meV scale and move apart with increasing field strength. This can be a possibility to fine tuning the absorbed energy. In the limiting case of vanishing magnetic field the final excited levels merge in pairs and form the second and third level, respectively, thus in the absence of the field one should expect two identical transitions from the ground state to those levels irrespective of polarization type.

Excitations induced by both polarization types depend in a similar manner on side thickness and thus below we focus only on the effects induced by clockwise polarized electromagnetic field which excites the ground state electron to the third and ninth energy levels [the green solid lines in Fig. 6]. The first absorption peak is centered around the energy defined by the difference between the third and the first energy levels while the second maximum is formed at the energy equal to the splitting of the ninth and the ground level. The external magnetic field lifts the energy level degeneracy, but all of the levels which in the absence of that field form one degenerate level change similarly with side thickness. In particular, the two lowest levels decay with increasing thickness like the ground state in the absence of the field [the red line in Fig. 2(b)] while the levels from seventh to tenth decrease like the third level of the degenerate system [the blue line in Fig. 2(b)]. As a result the positions of the two absorption peaks change with side thickness similarly to the splittings of the relevant degenerate levels [Fig. 2(c)].

The energy difference between the ground state and the third excited level increases with side thickness

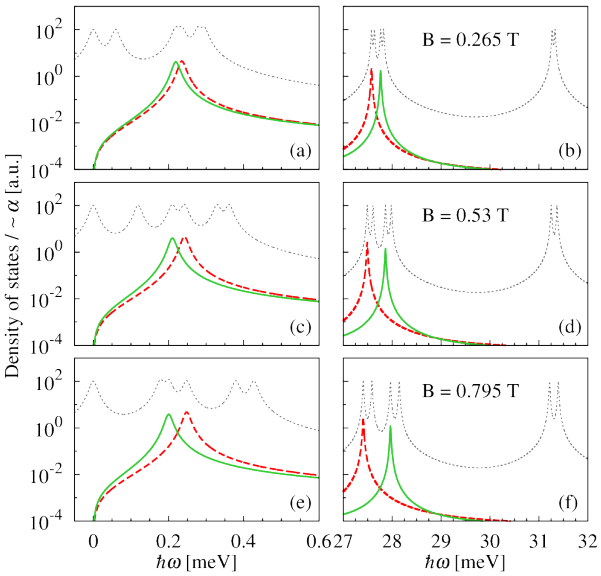

Figure 6: Absorption coefficients associated with clockwise (green solid) and counterclockwise (red dashed) polarization superimposed on the density of states (gray dotted) for a 12 nm thick equilateral ring obtained in the presence of external magnetic field. Values of the field shown in the right panels refer also to the left ones. Figs. (a), (c) and (e) show transitions from the ground state to other corner-localized states while Figs. (b), (d) and (f) transitions to side-localized states. For visibility we use a logarithmic scale for the absorption functions.

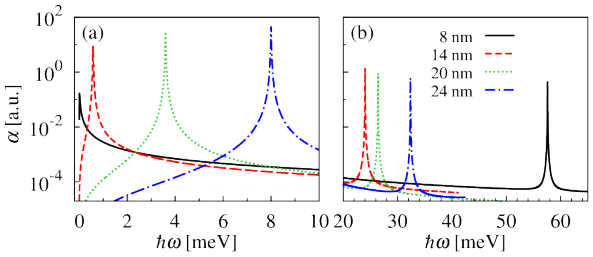

Figure 7: Absorption coefficients associated with clockwise polarization and excitations from the ground state to other corner- (a) and side-localized (b) states of equilateral triangular rings of different side thickness d. Values shown in Fig. (b) refer to both panels. $B = 0.53$ T. For visibility we use a logarithmic scale for the absorption functions.

and thus absorption maxima associated with this transition [Fig. 7(a)] move to higher energies. The energy interval which defines the position of the second peak depends on side thickness like the splitting between the third and ground levels of degenerate systems [blue dotted line in Fig. 2(c)]. Corner- and side-localized states of thin triangular rings are separated from each other by a large energy gap, as a consequence the splitting between the ground state and the first optically accessible side-localized state is also considerably large and thus the second absorption peak occurs at high energies [the black solid line in Fig. 7(b)]. With increasing side thickness the relevant energy splitting decreases, as a result the second absorption peak initially shifts to lower energies. The situation changes when the aspect ratio corresponding to the minimal difference between the initial and final levels is reached. From this point the absorption maximum moves back to higher energies, because the energy difference between the ground state and the ninth level increases with side thickness for sufficiently thick samples, Fig. 7(b).

This means that it is possible to achieve two rings for which aspect ratios differ considerably but the samples still have one transition induced by photons of the same frequency. Irrespective of the sample shape the first transition requires absorption of electromagnetic waves from the THz region. On the contrary, excitations to the side-localized states show much stronger dependence on the sample geometry and may be produced by THz and infrared electromagnetic waves as well. This shows that the absorption spectrum of triangular quantum rings may cover wide range of wavelengths and may be engineered during the manufacturing process through side thickness and then, more precisely, by external magnetic or electric fields.

In the case of equilateral rings (Fig. 7) the absorption coefficients associated with both transitions differ

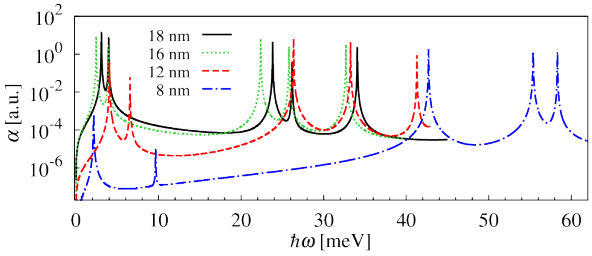

Figure 8: Absorption coefficients associated with clockwise polarization and excitations from the ground state to the first five excited levels of non-symmetric samples, defined in Figs. 4 and 5. The numbers shown in the figure refer to the thickness of the narrowest sides, $B = 0$. For visibility we use a logarithmic scale for the absorption functions.

up to one order of magnitude throughout the whole range of analyzed side thicknesses. This situation does not hold for non-symmetric samples. The absorption coefficients (Eq. 3) depend on energy gaps and on dipole moments. The former ones change similarly in both cases [Figs. 2(c) and 4(c)], but wave functions [localization shown in Figs. 3 and 5] and thus dipole moments are very sensitive to the sample symmetry. As a result the absorption spectrum of non-symmetric rings (Fig. 8) differs considerably from the one of equilateral samples (Fig. 7). The first consequence of the broken wave function symmetry is the increased number of optically induced transitions. In principle all spin-allowed excitations occur, i.e., the ground state electron may be excited to the two higher levels associated with localization in corner areas and to the three levels corresponding to mostly side-localized probability distributions (Fig. 8). Moreover this occurs in the presence of both polarization types. The positions of the absorption peaks are determined by the energy intervals between the ground state and the five excited levels [Fig. 4(a)] and change with side thickness. For example, the position of the first absorption peak is determined by the energy separation between the second energy level and the ground state while the third maximum occurs for energy equal to the difference between the third and first levels. The energies at which those two absorption peaks built up depend on side thickness like the green and blue lines in Fig. 4(c), respectively Thin samples absorb much stronger photons of higher frequencies which allow for excitation of the ground state electrons (localized around a single corner) to states associated with probability distributions forming single maxima in the middle of each side. For such samples the absorption in the corner-state domain in negligibly small. The absorption coefficients corresponding to transitions to other corner-localized states constantly increase with ring thickness such that for thick samples they exceed the ones occurring at higher frequencies. The strong dependence of the absorption coefficient on aspect ratio suggests that samples with different optical properties may be relatively easily obtained by slightly changing the deposition time during the fabrication of the core-shell structure.

4 Conclusions

We studied how sample geometry details affect energy levels and the corresponding probability distributions of a single electron confined in a triangular quantum ring. We also showed how those features determine optical absorption of circularly polarized electromagnetic field. The ground state of triangular samples restricted internally and externally by regular polygons is twofold degenerate and is followed by alternating sequence of pairs of four- and twofold degenerate levels. The energy degeneracy depends only on the ring symmetry and the fourfold degenerate levels may be split into pairs of spin degenerate eigenvalues if the symmetry is broken by, e.g., different side thicknesses. The spin degeneracy is lifted when the sample is immersed in external magnetic field. The splittings between consecutive levels strongly depend on aspect ratio. If the external radius is assumed to be constant then, the separations between the ground state and all other states associated with corner-localized probability distributions increases with side thicknesses. The main energy gap which separates corner- from side-localized states decreases with the side thickness until the lowest energy gap, occurring for the aspect ratio of about 0.34, is reached and then the gap increases slightly again. Contrary to other polygonal rings, in the case of triangular samples this gap is always considerably larger than the energy splittings in the corner state domain. The position of the ground state, followed by the excited levels, is shifted to lower energies with increasing side thickness. Electron localization is also very sensitive to the sample shape. Low-energy electrons confined in thin rings occupy only very small corner areas, with increasing side thickness the corresponding localization peaks penetrate into side areas and overlap. The probability distributions associated with energy levels above the main gap change in the opposite way, i.e., wide peaks spread along side areas become sharper with increasing aspect ratio and for sufficiently thick rings are accompanied by lower maxima formed around corner areas.

The energy levels and corresponding wave functions govern absorption spectrum of the systems. The positions of absorption peaks are determined by energy splittings between pairs of particular levels, while their amplitudes depend on dipole moments and thus on wave functions. As a result the energy of absorbed electromagnetic field depends on sample shape. Since the corner- and side-localized states are always separated by a considerable energy gap, excitations of an electron from the ground state to other corner-localized states and side-localized states occurs in the presence of photons associated with wavelengths belonging to different electromagnetic domains. Thus, by selecting the appropriate ring thickness and shape, one can engineer the absorption in the THz and in the infrared domain.

For simplicity of description and discussion we keep the external radius constant and change only the side thickness. The way how the energy levels change does not depend on the ring diameter but only on the aspect ratio between the side thickness and the external radius. Nonetheless energy levels of nanoscale systems do depend on sample sizes, and thus the results shown in Fig. 2 calculated for different external radii would look the same, but the axes would be scaled differently.

Throughout this work the electron-electron Coulomb interaction was neglected. Strictly speaking the results presented correspond to transitions of a single electron in the triangular ring. As long as the Coulomb interaction is small, possibly due to a large dielectric constant of the material, its main effect is a renormalization of the energy spectrum. However, because of the small energy dispersion of the corner states, non-trivial Coulomb effects could be expected.

Acknowledgement

This work was mainly supported by the Research Fund of the University of Iceland. Additional funding from the Nordic network NANOCONTROL, project No.: P-13053, and COST Action MP1204 'Tera-MIR Radiation: Materials, Generation, Detection and Applications' is acknowledged.

References

[1] Shi T, Jackson H E, Smith L M, Jiang N, Gao Q, Tan H H, Jagadish C, Zheng C and Etheridge J 2015 *Nano Letters* **15** 1876–1882 pMID: 25714336 (*Preprint* http://dx.doi.org/10.1021/nl5046878) URL http://dx.doi.org/10.1021/nl5046878

[2] Krogstrup P, Jorgensen H I, Heiss M, Demichel O, Holm J V, Aagesen M, Nygard J and Fontcuberta i Morral A 2013 *Nature Photonics* **7** 306–310 URL http://dx.doi.org/10.1038/nphoton.2013.32

[3] Tang J, Huo Z, Brittman S, Gao H and Yang P 2011 *Nature Nanotechnology* **6** 568–572 URL http://dx.doi.org/10.1038/nnano.2011.139

[4] Kim S K, Zhang X, Hill D J, Song K D, Park J S, Park H G and Cahoon J F 2015 *Nano Letters* **15** 753–758 pMID: 25546325 (*Preprint* http://dx.doi.org/10.1021/nl504462e) URL http://dx.doi.org/10.1021/nl504462e

[5] Xiang J, Lu W, Hu Y, Wu Y, Yan H and Lieber C M 2006 *Nature* **441** 489–493

[6] Nguyen B M, Taur Y, Picraux S T and Dayeh S A 2014 *Nano Letters* **14** 585–591 (*Preprint* http://pubs.acs.org/doi/pdf/10.1021/nl4037559) URL http://pubs.acs.org/doi/abs/10.1021/nl4037559

[7] Saxena D, Mokkapati S, Parkinson P, Jiang N, Gao Q, Tan H H and Jagadish C 2013 *Nat Photon* **7** 963–968 URL http://dx.doi.org/10.1038/nphoton.2013.303

[8] Ho J, Tatebayashi J, Sergent S, Fong C F, Iwamoto S and Arakawa Y 2015 *ACS Photonics* **2** 165–171 (*Preprint* http://dx.doi.org/10.1021/ph5003945) URL http://dx.doi.org/10.1021/ph5003945

[9] Thierry R, Perillat-Merceroz G, Jouneau P H, Ferret P and Feuillet G 2012 *Nanotechnology* **23** 085705 URL http://stacks.iop.org/0957-4484/23/i=8/a=085705

[10] John Ibanes J, Herminia Balgos M, Jaculbia R, Salvador A, Somintac A, Estacio E, Que C T, Tsuzuki S, Yamamoto K and Tani M 2013 *Applied Physics Letters* **102** 063101 URL http://scitation.aip.org/content/aip/journal/apl/102/6/10.1063/1.4791570

[11] Peng K, Parkinson P, Fu L, Gao Q, Jiang N, Guo Y N, Wang F, Joyce H J, Boland J L, Tan H H, Jagadish C and Johnston M B 2015 *Nano Letters* **15** 206–210 pMID: 25490548 (*Preprint* http://dx.doi.org/10.1021/nl5033843) URL http://dx.doi.org/10.1021/nl5033843

[12] Chuang S L 1995 *Physics of Optoelectronic Devices* (New York: John Wiley and Sons, Inc.)

[13] Pistol M E and Pryor C E 2008 *Phys. Rev. B* **78**(11) 115319 URL http://link.aps.org/doi/10.1103/PhysRevB.78.115319

[14] Wong B M, Léonard F, Li Q and Wang G T 2011 *Nano Letters* **11** 3074–3079 pMID: 21696178 (*Preprint* http://dx.doi.org/10.1021/nl200981x) URL http://dx.doi.org/10.1021/nl200981x

[15] Blömers C, Rieger T, Zellekens P, Haas F, Lepsa M I, Hardtdegen H, Gül Ö, Demarina N, Grützmacher D, Lüth H and Schäpers T 2013 *Nanotechnology* **24** 035203 URL http://stacks.iop.org/0957-4484/24/i=3/a=035203

[16] Rieger T, Luysberg M, Schäpers T, Grützmacher D and Lepsa M I 2012 *Nano Letters* **12** 5559–5564 pMID: 23030380 (*Preprint* http://dx.doi.org/10.1021/nl302502b) URL http://dx.doi.org/10.1021/nl302502b

[17] Haas F, Sladek K, Winden A, von der Ahe M, Weirich T E, Rieger T, Lüth H, Grützmacher D, Schäpers T and Hardtdegen H 2013 *Nanotechnology* **24** 085603 URL http://stacks.iop.org/0957-4484/24/i=8/a=085603

[18] Sprung D W L, Wu H and Martorell J 1992 *J. Appl. Phys.* **71**(1) 515–517

[19] Ballester A, Planelles J and Bertoni A 2012 *Journal of Applied Physics* **112** 104317 URL http://scitation.aip.org/content/aip/journal/jap/112/10/10.1063/1.4766444

[20] Sitek A, Serra L, Gudmundsson V and Manolescu A 2015 *Phys. Rev. B* **91**(23) 235429 URL http://link.aps.org/doi/10.1103/PhysRevB.91.235429

[21] Estarellas C and Serra L 2015 *Superlattice Microstruct* **83** 184

[22] Daday C, Manolescu A, Marinescu D C and Gudmundsson V 2011 *Phys. Rev. B* **84**(11) 115311 URL http://link.aps.org/doi/10.1103/PhysRevB.84.115311

[23] Groth C W, Wimmer M, Akhmerov A R and Waintal X 2014 *New Journal of Physics* **16** 063065 URL http://stacks.iop.org/1367-2630/16/i=6/a=063065

[24] Haug H and Koch S W 2009 *Quantum Theory of the Optical and Electronic Properties of Semiconductors* 5th ed (Singapore: World Scientific)

[25] Hu H, Zhu J L and Xiong J J 2000 *Phys. Rev. B* **62**(24) 16777–16783 URL http://link.aps.org/doi/10.1103/PhysRevB.62.16777